

Communication

Cure Kinetics of Samarium-Doped Fe₃O₄/Epoxy Nanocomposites

Maryam Jouyandeh ¹, Mohammad Reza Ganjali ^{1,2,3}, Mehdi Mehrpooya ⁴, Otman Abida ⁵, Karam Jabbour ⁵, Navid Rabiee ⁶, Sajjad Habibzadeh ⁷, Amin Hamed Mashahdzadeh ⁸, Alberto García-Peñas ^{9,10}, Florian J. Stadler ^{9,*} and Mohammad Reza Saeb ^{11,*}

- ¹ Center of Excellence in Electrochemistry, School of Chemistry, University of Tehran, Tehran 14176-14411, Iran; maryam.jouyandeh@gmail.com (M.J.); ganjali@ut.ac.ir (M.R.G.)
 - ² School of Resources and Environment, University of Electronic Science and Technology of China, Chengdu 611731, China
 - ³ Biosensor Research Center, Endocrinology and Metabolism Molecular-Cellular Sciences Institute, Tehran University of Medical Sciences, Tehran 14117-13137, Iran
 - ⁴ Department of Renewable Energies and Environment, Faculty of New Sciences and Technologies, University of Tehran, Tehran 14155-6619, Iran; mehrpoya@ut.ac.ir
 - ⁵ College of Engineering and Technology, American University of the Middle East, P.O. Box 220, Dasman 15453, Kuwait; otman.abida@aum.edu.kw (O.A.); karam.jabbour@aum.edu.kw (K.J.)
 - ⁶ Department of Physics, Sharif University of Technology, Tehran 11155-9161, Iran; nrabiee94@gmail.com
 - ⁷ Department of Chemical Engineering, Amirkabir University of Technology (Tehran Polytechnic), Tehran 15916-34311, Iran; sajjad.habibzadeh@aut.ac.ir
 - ⁸ Mechanical and Aerospace Engineering, School of Engineering and Digital Sciences, Nazarbayev University, Nur-Sultan 010000, Kazakhstan; amin.hamed.m@gmail.com
 - ⁹ College of Materials Science and Engineering, Guangdong Research Center for Interfacial Engineering of Functional Materials, Nanshan District Key Laboratory for Biopolymers and Safety Evaluation, Shenzhen Key Laboratory of Polymer Science and Technology, Lihu Campus, Shenzhen University, Shenzhen 518055, China; alberto.garcia.penas@uc3m.es
 - ¹⁰ Departamento de Ciencia e Ingeniería de Materiales e Ingeniería Química (IAAB), Universidad Carlos III de Madrid, 28911 Leganés, Spain
 - ¹¹ Department of Polymer Technology, Gdańsk University of Technology, G. Narutowicza 11/12, 80-233 Gdańsk, Poland
- * Correspondence: fjstadler@szu.edu.cn (F.J.S.); mrsaeb2008@gmail.com (M.R.S.)



Citation: Jouyandeh, M.; Ganjali, M.R.; Mehrpooya, M.; Abida, O.; Jabbour, K.; Rabiee, N.; Habibzadeh, S.; Mashahdzadeh, A.H.; García-Peñas, A.; Stadler, F.J.; et al. Cure Kinetics of Samarium-Doped Fe₃O₄/Epoxy Nanocomposites. *J. Compos. Sci.* **2022**, *6*, 29. <https://doi.org/10.3390/jcs6010029>

Academic Editor:
Francesco Tornabene

Received: 6 December 2021

Accepted: 8 January 2022

Published: 17 January 2022

Publisher's Note: MDPI stays neutral with regard to jurisdictional claims in published maps and institutional affiliations.



Copyright: © 2022 by the authors. Licensee MDPI, Basel, Switzerland. This article is an open access article distributed under the terms and conditions of the Creative Commons Attribution (CC BY) license (<https://creativecommons.org/licenses/by/4.0/>).

Abstract: To answer the question “How does lanthanide doping in iron oxide affect cure kinetics of epoxy-based nanocomposites?”, we synthesized samarium (Sm)-doped Fe₃O₄ nanoparticles electrochemically and characterized it using Fourier-transform infrared spectroscopy (FTIR), X-ray powder diffraction (XRD), field emission scanning electron microscopy (FE-SEM), energy dispersive X-Ray analysis (EDX), transmission electron microscopy (TEM), and X-ray photoelectron spectroscopy analyses (XPS). The magnetic particles were uniformly dispersed in epoxy resin to increase the curability of the epoxy/amine system. The effect of the lanthanide dopant on the curing reaction of epoxy with amine was explored by analyzing differential scanning calorimetry (DSC) experimental data based on a model-free methodology. It was found that Sm³⁺ in the structure of Fe₃O₄ crystal participates in cross-linking epoxy by catalyzing the reaction between epoxide rings and amine groups of curing agents. In addition, the etherification reaction of active OH groups on the surface of nanoparticles reacts with epoxy rings, which prolong the reaction time at the late stage of reaction where diffusion is the dominant mechanism.

Keywords: lanthanide; samarium (Sm)-doped Fe₃O₄ nanoparticles; epoxy coating; curing reaction

1. Introduction

The subject of magnetic nanoparticles has attracted significant interest, in particular, in the medical field and other high-tech applications [1–3]. Magnetite nanoparticle-filled

polymers have been widely used in various applications such as electronic devices, nonlinear optic systems, sensors, magnetic filters, and photovoltaic solar cells [4]. Owing to their good properties and low price, magnetite (Fe_3O_4) nanoparticles have been studied most among the various kinds of magnetic nanoparticles [5–7].

Fe_3O_4 nanoparticles have been used in epoxy matrices to improve their final properties [8]. Dispersion state and interfacial interaction between Fe_3O_4 nanoparticles and epoxy matrix are two important parameters that affect the cross-linking reaction and final properties of epoxy nanocomposites [9,10]. Homogenous dispersion of nanoparticles in an epoxy matrix and strong interfacial interaction between Fe_3O_4 nanoparticles and polymer matrix are required to achieve a dense crosslinked network with improved final properties, in particular, in terms of mechanical performance [11,12]. However, magnetite nanoparticles have a high tendency to aggregate in the epoxy matrix [13]. It was shown that the success in curing the reaction of epoxy is highly dependent on the dispersibility of Fe_3O_4 nanoparticles in the resin matrix. However, the possibility of unmodified Fe_3O_4 nanoparticles to form agglomerates is high, hindering cross-linking reactions [14]. Many research works revealed that surface functionalization of Fe_3O_4 nanoparticles results in well-dispersed nanoparticles in the epoxy matrix [15,16]. Recently, it was shown that bulk modification of Fe_3O_4 nanoparticles by doping other metal ions can strongly affect cross-linking reaction of epoxy [17–19]. Furthermore, with an eye to possibly to enhance the properties of the Fe_3O_4 nanoparticles, doping of magnetite nanoparticles with other metal ions has been explored [20,21].

Lanthanides feature an f-electron shell, a property that only very heavy atoms have, which gives them unique optical and magnetic properties, making them interesting as dopants for other nanoparticles [22]. Besides introducing new properties, the doping of magnetite particles with small amounts of lanthanides leads to only minor alterations of physical and chemical characteristics. The doping of other metals/metal ions, such as zinc, manganese, copper, nickel, and cobalt, into the Fe_3O_4 nanoparticles enhances the availability of its surface sites [23–25]. Among lanthanides, samarium (Sm) has high magnetic properties and is relatively stable at room temperature. This rare-earth element is used in many applications such as microwave, electronic devices, optical lasers, and neutron absorbers in nuclear reactors [26,27]. Doping Fe_3O_4 nanoparticles with Sm atoms can increase the number of surface active sites and surface area of base nanoparticles, which may enhance the curability of epoxy resin. To the best of our knowledge, the effect of Sm-doped Fe_3O_4 nanoparticles on the curing reaction of epoxy resin has not been studied until now.

In the present study, Sm-doped Fe_3O_4 nanoparticles were fabricated via an electrochemical method. The synthesized samples were well characterized by Fourier-transform infrared spectroscopy (FTIR), X-ray powder diffraction (XRD), field emission scanning electron microscopy (FE-SEM), energy dispersive X-ray analysis (EDX), transmission electron microscopy (TEM), and X-ray photoelectron spectroscopy analyses (XPS). Then, the epoxy-based film was reinforced with Sm-doped Fe_3O_4 nanoparticles to obtain an excellent corrosion protection coating. The cure potential of the epoxy-containing Sm-doped Fe_3O_4 nanoparticles was evaluated with dynamic differential scanning calorimetry (DSC) at different heating rates of 2.5, 5, 7.5, and 10 °C/min.

2. Materials and Methods

Iron (II) chloride ($\text{FeCl}_2 \cdot 4\text{H}_2\text{O}$), iron(III) nitrate nonahydrate 99.9% ($\text{Fe}(\text{NO}_3)_3 \cdot 9\text{H}_2\text{O}$), and samarium(III) nitrate ($\text{Sm}(\text{NO}_3)_3 \cdot (\text{H}_2\text{O})_2$) were supplied by Sigma-Aldrich. Araldite LY 5052 epoxy resin and HY 5052 curing agent were purchased from MIS Hindustan Ciba-Geigy.

2.1. Synthesis of Sm-Doped Fe_3O_4 Nanoparticles

Sm^{3+} -doped Fe_3O_4 nanoparticles were prepared through the cathodic electrodeposition (CED) procedure using a stainless steel cathode (316 L, 5 cm × 5 cm × 0.5 mm) inside

two graphite anodes. The electrolyte 0.005 molar solution of iron(III) nitrate nonahydrate (2 g), iron(II) chloride (1 g), and samarium(III) nitrate (0.6 g) was prepared in water. Then, deposition occurred using a Potentiostat/Galvanostat, Model: NCF-PGS 2012 (Metrohm Autolab) at 25 °C and current density of 10 mA cm⁻² for 30 min followed by rinsing with deionized water several times. Finally, the dispersed Sm-Fe₃O₄ deposit in deionized water was centrifuged at 6000 rpm for 20 min, separated, and dried at 70 °C for 1 h.

2.2. Preparation of Epoxy/Sm-Doped Fe₃O₄ Nanocomposite

Epoxy nanocomposites were obtained by mixing 0.1 wt.% of Sm-doped Fe₃O₄ using a mechanical mixer at 2500 rpm for 15 min. Then, Sm-doped Fe₃O₄ in epoxy was further mixed by sonication for 5 min. Finally, the curing agent was added to EP/Sm-Fe₃O₄ nanocomposite in the stoichiometric ratio of 38/100 (curing agent/epoxy).

2.3. Characterization

The FTIR spectrum of Sm-doped Fe₃O₄ nanoparticles was obtained by Bruker Vector spectrometer, Coventry, UK, between 4000–400 cm⁻¹ wavelength. X-ray diffraction (XRD) of nanoparticles was performed by a Philips PW-1800 apparatus (Amsterdam, Netherlands) with Co K α radiation. The micro- and nano-images of Sm-Fe₃O₄ nanoparticles were obtained by FESEM and EDX-Mapping (Mira 3-XMU, TESCAN, Brno-Kohoutovice, Czech Republic) at the voltage of 100 kV and TEM (Zeiss-EM10C-80 kV, Jena, Germany). A Thermo Fisher Scientific instrument XPS elemental analyzer (Waltham, MA, USA) determined the X-ray Photoelectron Spectroscopic properties of the nanoparticles.

The cure reaction of neat epoxy and EP/Sm-Fe₃O₄ nanocomposite was investigated by analyzing 12 mg of each sample using DSC (Perkin Elmer, DSC 4000, Waltham, MA, USA) at four different heating rates (2.5, 5, 7.5 and 10 °C·min⁻¹) in the temperature range of 15–300 °C under nitrogen atmosphere.

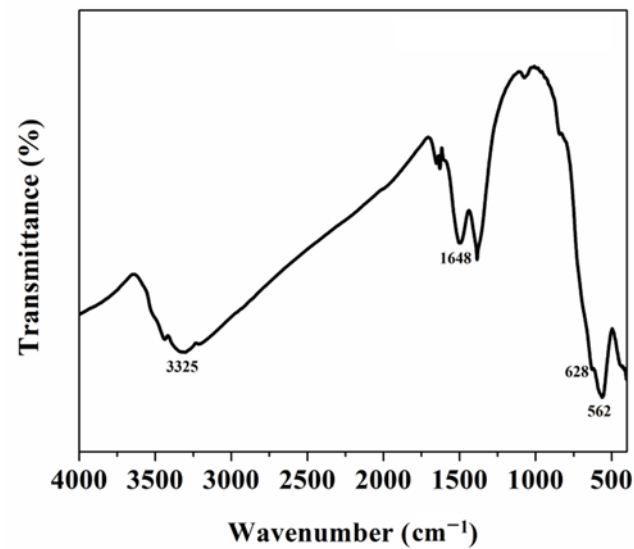
3. Results and Discussion

3.1. Characterization of Sm-Fe₃O₄ Nanoparticles

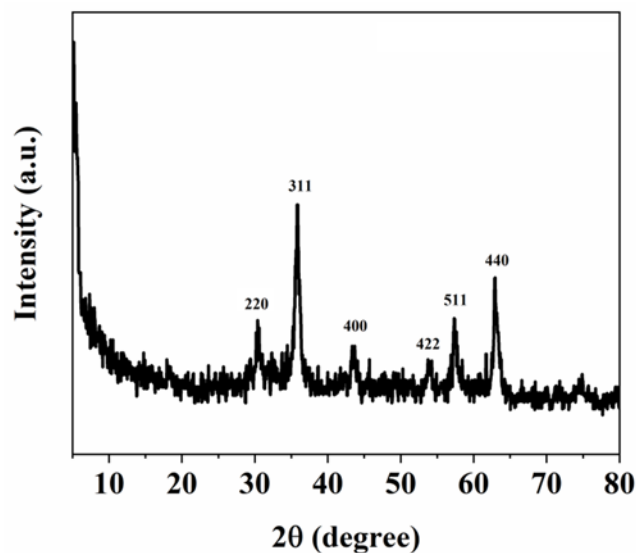
The FTIR spectrum of the prepared Sm-Fe₃O₄ nanoparticle is shown in Figure 1a. Two sharp bands can be observed at 562 cm⁻¹ and 628 cm⁻¹, which are ascribed to the splitting of the ν_1 band of the Fe–O. A wide peak in the range of 415–443 cm⁻¹ is due to ν_2 bands of the Fe–O and Sm–O [26]. The appearance of bands at 1648 and 3325 cm⁻¹ are attributed to the stretching and deformation vibrations of O–H groups on the surface of Sm-Fe₃O₄ nanoparticles.

Figure 1b shows the XRD pattern of Sm-Fe₃O₄ nanoparticles, which is the cubic spinel structure of Magnetite Fe₃O₄ [Joint Committee on Powder Diffraction Standards (JCPDS) 76-1849 and Inorganic Crystal Structural Database (ICSD) 28664]. A significant change was not observed in the XRD patterns of doped nanoparticles. The XRD pattern shows that doping Sm does not change the crystal structure of Fe₃O₄ nanoparticles.

The oxygen atoms in magnetite (Fe₃O₄) form an inverse Spinel structure—a close-packed face-centered cubic sublattice, where Fe(II) are located in the octahedral sites and Fe(III) are occupying octahedral and tetrahedral sites [28], which can be described by (Fe₈³⁺)^{tetr}[Fe³⁺Fe²⁺]₈^{oct}O₃₂. The close-packed plane is along the (111) axis, occupied by oxygen atoms. Those sites can also be occupied by the transition metal atoms [29]. Samarium ions, similarly to other lanthanide(III) ions, have six coordination sites and seven octahedral coordination sites, when crystallizing as Sm₂O₃ [30], making them suitable for being included in the inverse spinel structure at the octahedral sites.



(a)



(b)

Figure 1. (a) FTIR spectra of Ce-doped Fe₃O₄ and (b) XRD pattern of Sm-doped Fe₃O₄.

Figure 2 shows the FESEM, EDS, mapping, and TEM images of Sm-Fe₃O₄ nanoparticles. The average particle size is about 20 nm. The EDX experiments proved the presence of nanoparticles, containing both Fe and Sm at approximately equal amounts (Figure 2b). Additionally, O (25.4%) and Au were found, the latter stemming from the TEM grids used.

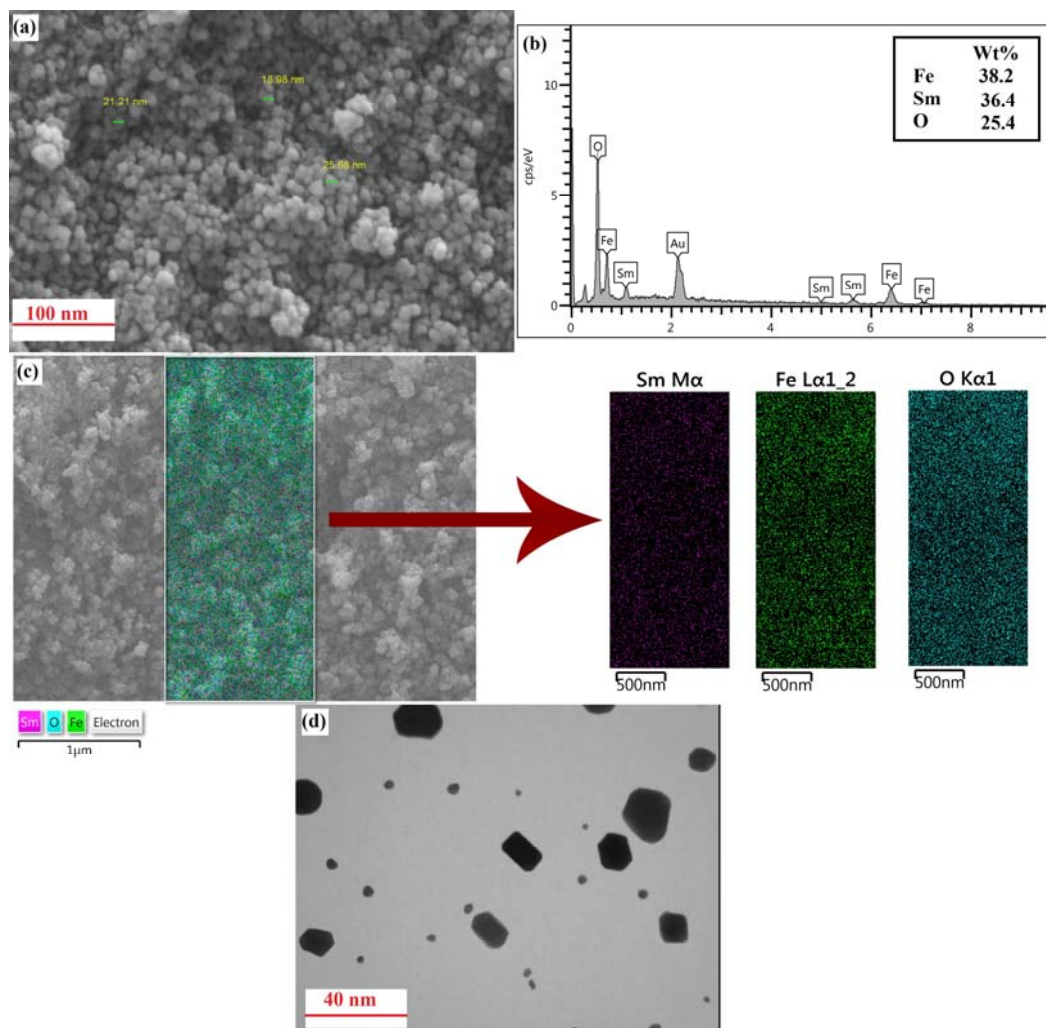


Figure 2. (a) FESEM, (b) EDX, (c) elemental mapping and (d) TEM of Sm-doped Fe_3O_4 .

The presence of Fe and Sm, O, and C in the Sm- Fe_3O_4 nanoparticles is confirmed by XPS analysis (Figure 3a), as the Fe2p peaks (Figure 3b) are clearly visible in terms of Fe2p_{1/2} (710 eV) and Fe2p_{3/2} peaks (720 eV), confirming the Fe(III)-oxidation state [31]. The Fe(II) in Fe_3O_4 is confirmed by the shoulder at 708 eV (Fe2p_{1/2} peak) and at 721 eV (Fe2p_{3/2} peak) [32].

Sm-3d_{5/2} regions of Sm- Fe_3O_4 nanoparticles are shown in Figure 3c. The binding energy values (3d_{5/2}) of Sm(III) (1079 and 1107 eV) observed in the nanoparticles are in accordance with the standard values [Sm_2O_3 (1082 and 1108 eV) [33], thus this lanthanide is in its +3 oxidation state in Sm-doped Fe_3O_4 . The varied coordination conditions in the crystal structure could explain the subtle differences observed.

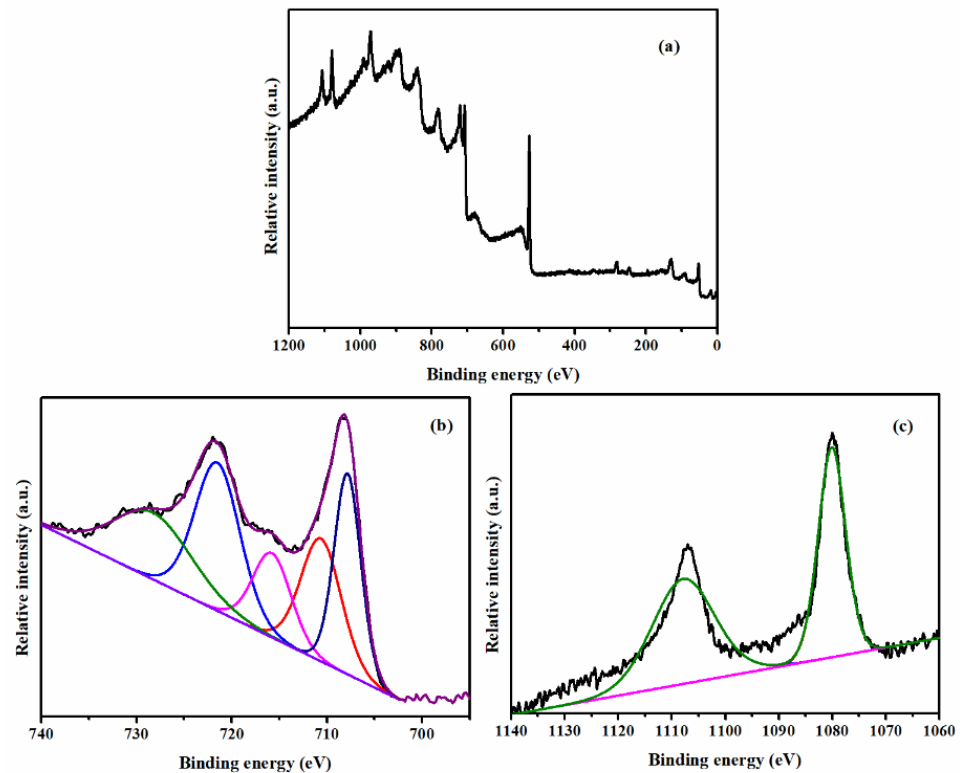


Figure 3. XPS spectra of the Sm-doped Fe_3O_4 (a) Survey, (b) Fe2p, and (c) Sm3d. Colored lines refer to the individual peak fits as explained in the text.

3.2. Curing Analysis

Figure 4 displays nonisothermal DSC thermographs of neat epoxy and EP/ $\text{Sm-Fe}_3\text{O}_4$ cured with a stoichiometric amount of amine curing agent at heating rates of 2.5, 5, 7.5, and 10 °C/min. One exothermic peak can be observed for both samples at different heating rates, which revealed that the presence of $\text{Sm-Fe}_3\text{O}_4$ nanoparticles in the epoxy matrix does not change the domination of the chemically controlled reaction mechanism [34,35].

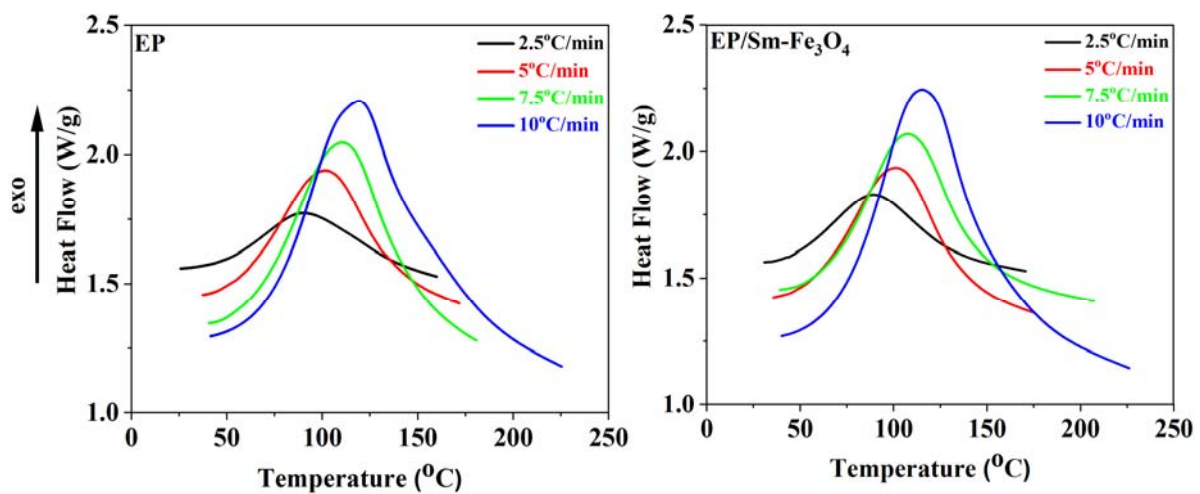


Figure 4. Dynamic DSC thermographs of EP and EP/ $\text{Sm-Fe}_3\text{O}_4$ at different heating rates.

The cure characteristics of EP and EP/ $\text{Sm-Fe}_3\text{O}_4$ nanocomposite include T_{Onset} , T_{Endset} , T_p , ΔT , and ΔH_∞ , which are the onset, endset, the exothermal peak temperature, temperature interval, and the enthalpy of complete cure, respectively, and are reported in Table 1.

T_{Onset} , T_{Endset} , and T_p shifted towards higher temperatures by increasing heating rates from 2.5 to 10 °C/min to compensate for reducing curing time [36,37].

Table 1. Cure characteristics of EP and EP/Sm-Fe₃O₄ nanocomposite as a function of heating rate.

Sample	Heating Rate (°C/min)	T_{Onset} (°C)	T_p (°C)	T_{Endset} (°C)	ΔT (°C)	ΔH_{∞} (J/g)	ΔT^*	ΔH^*	CI
EP	2.5	25.7	90.4	159.9	134.2	329.6	N.a.	N.a.	N.a.
	5.0	37.4	101.7	171.7	134.4	336.2	N.a.	N.a.	N.a.
	7.5	40.7	110.3	180.7	140.0	344.1	N.a.	N.a.	N.a.
	10	41.4	119.2	225.3	183.9	404.3	N.a.	N.a.	N.a.
EP/Sm-Fe ₃ O ₄	2.5	30.8	89.4	170.6	139.8	385.8	1.04	1.17	1.22
	5.0	35.7	101.5	175.2	139.5	363.7	1.04	1.08	1.12
	7.5	39.1	107.7	207.0	167.9	296.3	1.2	0.86	1.03
	10	40.1	115.1	226.0	185.9	403.4	1.01	1.01	1.02

N.a.: Not applicable.

The addition of Sm-Fe₃O₄ nanoparticles decreased T_{Onset} and T_p of epoxy/amine reaction, indicating that Sm doped magnetic nanoparticles accelerate cross-linking reaction. The surface activity of Sm-Fe₃O₄ nanoparticles can ascribe this increment in the system's reactivity due to the presence of Sm³⁺ in the crystal structure of nanoparticles that catalyze the reaction between epoxy and amine curing agents [23,38]. However, T_{Endset} , ΔT increased for EP/Sm-Fe₃O₄ nanocomposite compared to neat epoxy, which means that at the late stage of cure reaction, the OH groups on the surface of nanoparticles participate in etherification reaction and prolong the cross-linking of epoxy reaction.

The effect of the etherification reaction of OH groups on the surface of Sm-Fe₃O₄ nanoparticles as well as the catalyzing effect of Sm³⁺, which acts as Lewis acid, increase total heat of cure (ΔH_{∞}) of EP/Sm-Fe₃O₄ nanocomposite in comparison to neat epoxy (Figure 5) [39].

Figure 6 shows the conversion (α) of curing reaction as a function of temperature, which is obtained from Equation (1) [40]:

$$\alpha = \frac{\Delta H_T}{\Delta H_{\infty}}, \tag{1}$$

where ΔH_T is the enthalpy of reaction at a specific temperature.

In the initial stage of the curing reaction, cross-linking occurs rapidly until reaching gel point under the control of chemical reaction between the epoxy ring and amine groups of curing agent. In contrast, cross-linking occurs slowly at the late stage of cure, where diffusion is dominant. Additionally, Sm-Fe₃O₄ nanoparticles accelerate cross-linking of epoxy after vitrification, which indicated an acceleration of diffusion mechanisms due to the presence of OH groups on the nanoparticle surface [41].

Cure State of EP/Sm-Fe₃O₄

The effect of curability of Sm-Fe₃O₄ nanoparticles in epoxy/amine system are specified by Cure Index [42–44]:

$$CI = \Delta T^* \times \Delta H^*, \Delta T^* = \frac{\Delta T_{nanocomposite}}{\Delta T_{Reference}} \text{ and } \Delta H^* = \frac{\Delta H_{nanocomposite}}{\Delta H_{Reference}}, \tag{2}$$

ΔT is temperature window, within which curing occurs, with subscripts of “nanocomposite” and “Reference” for nanocomposite and blank epoxy systems, respectively. Similarly, ΔH_{∞} of such systems is defined. The terms with asterisks are dimensionless in each case. *Good*, *Poor*, and *Excellent* curing reactions of nanocomposites occur at $CI > \Delta H^*$, $CI < \Delta T^*$, and $\Delta T^* < CI < \Delta H^*$, respectively [45–47]. The addition of Sm-Fe₃O₄ nanoparticles in the epoxy matrix resulted in a *Good* cure reaction, which means that Sm³⁺ participates in cross-linking of epoxy by catalyzing the reaction between epoxide rings and amine groups of curing agents. In addition, the active OH groups on the surface of nanoparticles react with epoxy polar groups that increase both ΔT and ΔH and result in *Good* CI [48–50].

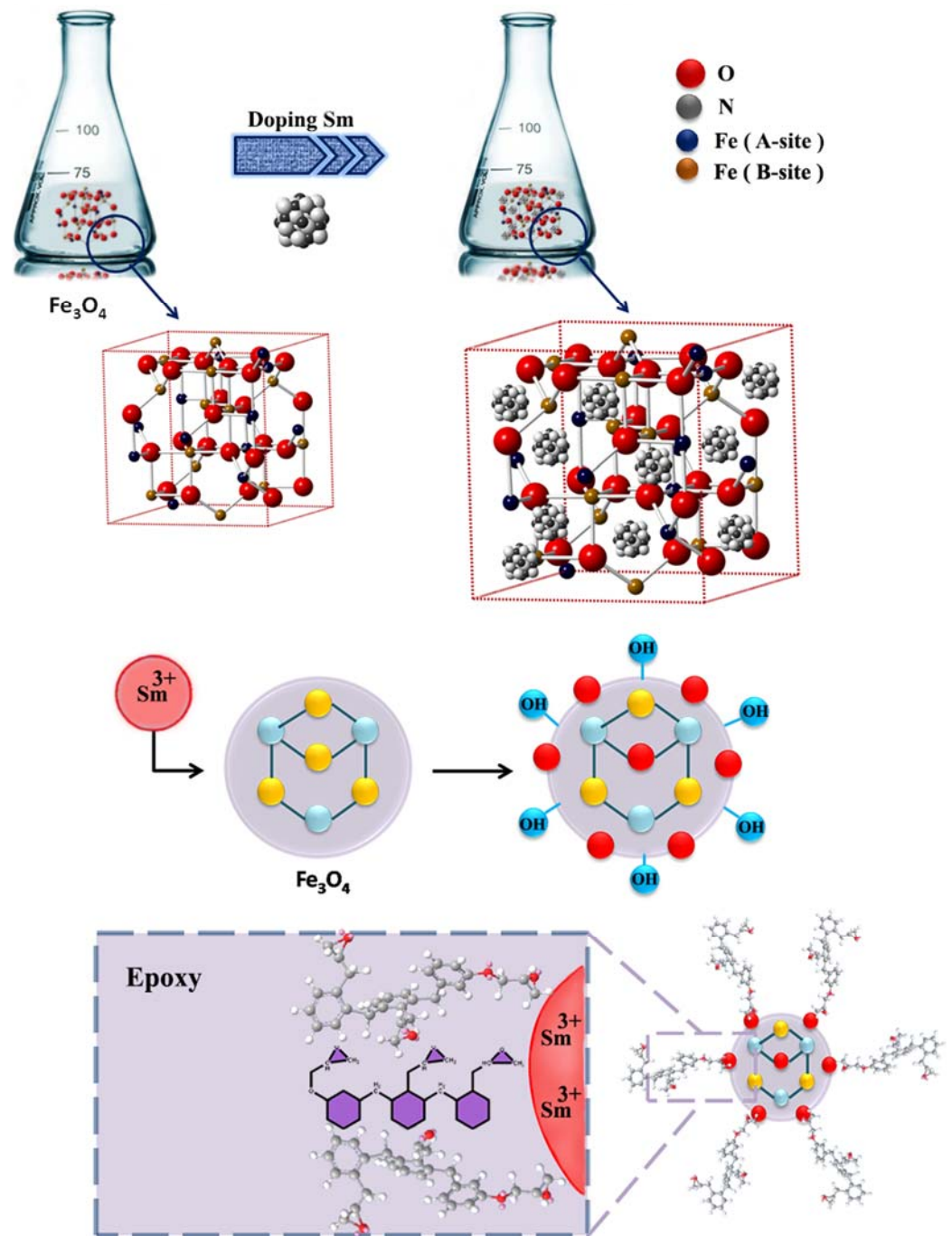


Figure 5. The schematic representation of synthesis Sm-Fe₃O₄ nanoparticles and its effect on the curing reaction of epoxy.

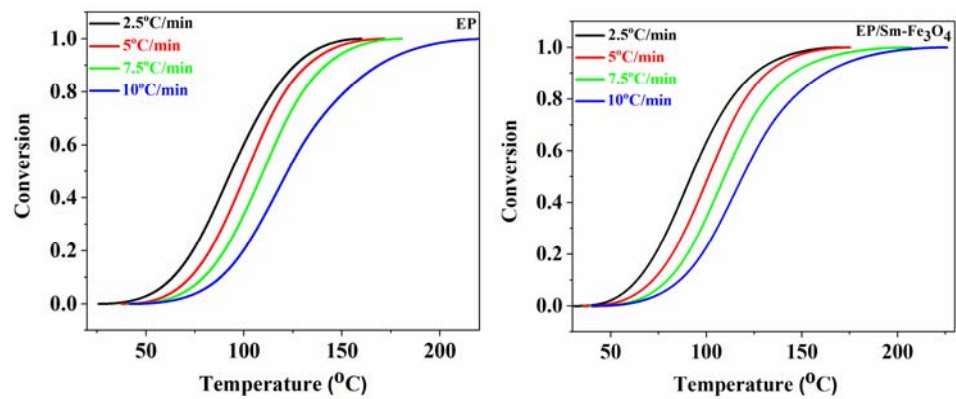


Figure 6. The fractional extent of conversion as a function of reaction time for EP and EP/Sm-Fe₃O₄ nanocomposite at heating rates of 2.5, 5, 7.5, and 10 °C/min.

3.3. Cure Kinetics of EP/Sm-Fe₃O₄

3.3.1. Calculation of Activation Energy

Isoconversional model-free Friedman (differential) and Kissinger–Akahira–Sunose (KAS, integral) were employed to obtain the apparent activation energies (E_α) of the curing reactions [51,52].

By plotting $\ln[\beta_i(d\alpha/dT)_{\alpha,i}]$ vs. $1/T_\alpha$ from Equation (3), the value of E_α is obtained from the slope of Figure 7a,b [53,54].

$$\ln \left[\beta_i \left(\frac{d\alpha}{dT} \right)_{\alpha,i} \right]_\alpha = \ln [f(\alpha) A_\alpha] - \frac{E_\alpha}{RT_{\alpha,i}} \quad (3)$$

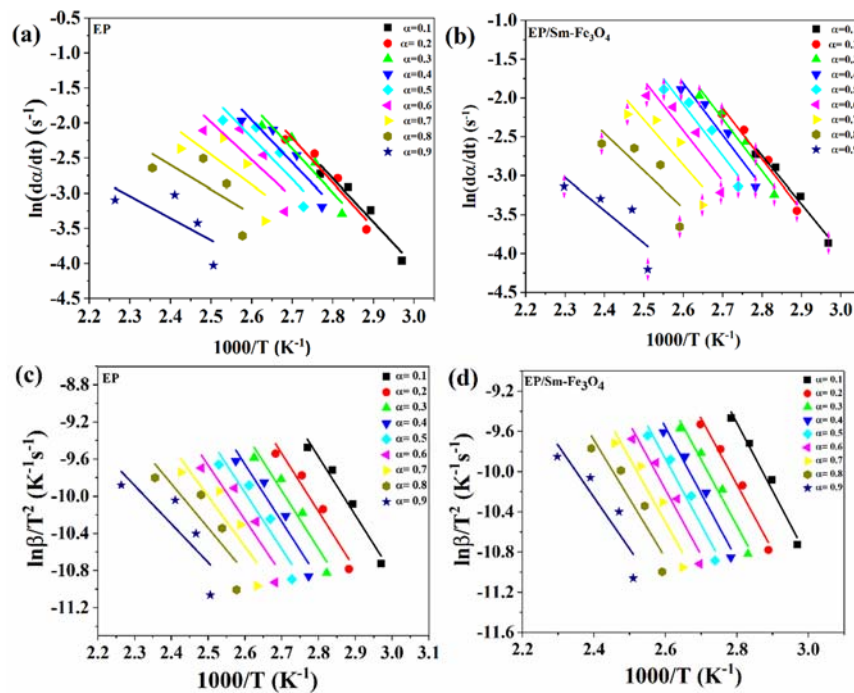


Figure 7. Friedman model plots of $\ln(d\alpha/dt)$ vs. $1/T$ for (a) EP and (b) EP/Sm-Fe₃O₄ nanocomposite and KAS model plots of $\ln(\beta/T^2)$ vs. $1/T$ for (c) EP and (d) EP/Sm-Fe₃O₄ nanocomposite at β of 2.5 °C/min.

Additionally, plotting $\ln\left(\beta_i/T_{\alpha,i}^2\right)$ vs. $1/T_\alpha$ from Equation (4) for each α value gives a value for the E_α (Figure 7c,d).

$$\ln\left[\frac{\beta_i}{T_{\alpha,i}^{1.92}}\left(\frac{d\alpha}{dT}\right)_{\alpha,i}\right]_\alpha = \text{Constant} - 1.0008\left(\frac{E_\alpha}{RT_{\alpha,i}}\right), \quad (4)$$

The apparent activation energy of neat epoxy and EP/Sm-Fe₃O₄ nanocomposite as a function of α based on both Friedman and KAS are shown in Figure 8. E_α was reduced for neat epoxy and its nanocomposite in α higher than 0.5 due to the participation of OH groups in epoxide ring-opening at a later stage of curing reaction revealing the autocatalytic mechanism of epoxy cure reaction [55,56]. The higher E_α values for EP/Sm-Fe₃O₄ nanocomposite compared to neat epoxy can be attributed to the higher viscosity of the epoxy system in the presence of Sm-Fe₃O₄ nanoparticles [57].

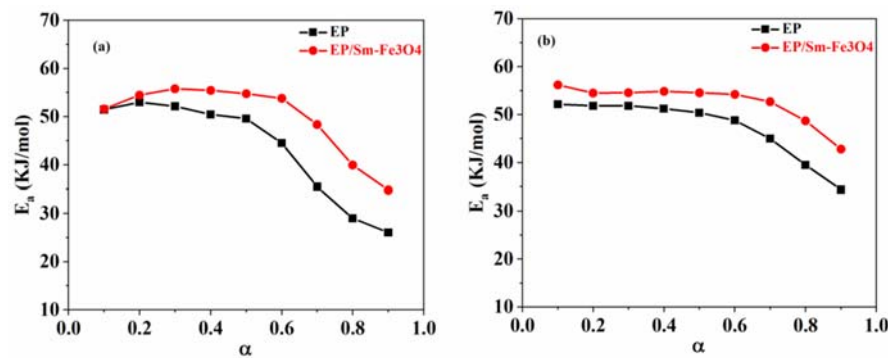


Figure 8. Evolution of activation energy for EP and EP/Sm-Fe₃O₄ nanocomposite estimated by (a) differential Friedman model and (b) integral KAS model.

3.3.2. Determination of Reaction Model

Friedman Model

The Friedman method can be used to show the non-catalytic or autocatalytic reaction model using Equation (5). The plot of $\ln[Af(\alpha)]$ vs. $\ln(1 - \alpha)$ shows a maximum in α between 0.2 and 0.4 that suggests an autocatalytic reaction mechanism (Figure 9) [58].

$$\ln[Af(\alpha)] = \ln\left(\frac{d\alpha}{dt}\right) + \frac{E}{RT} = \ln A + n\ln(1 - \alpha), \quad (5)$$

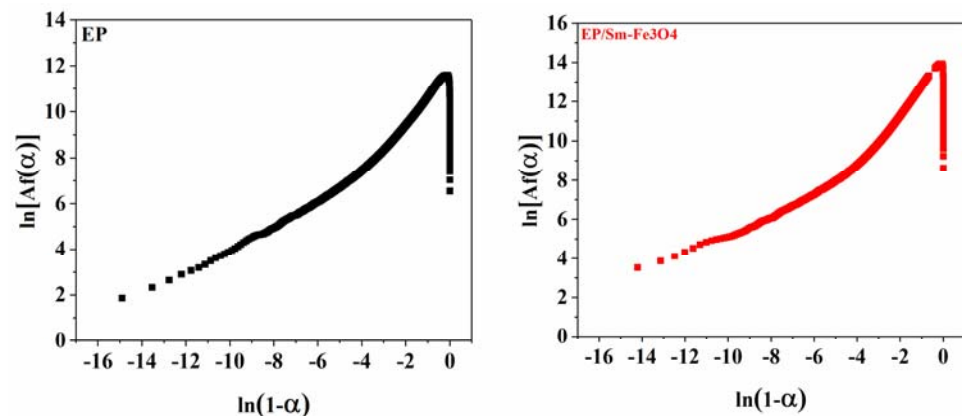


Figure 9. Plots of $\ln[Af(\alpha)]$ vs. $\ln(1 - \alpha)$ using Friedman model for EP and EP/Sm-Fe₃O₄ nanocomposite.

Malek Model

A more accurate Malek method was applied to determine the cross-linking reaction model through the shape and maximum points of $y(\alpha)$ and $z(\alpha)$ Malek master plots (Equations (6) and (7)) [59]. As can be observed in Figure 10 and Table 2, $\alpha_m = \text{Max}(y(\alpha))$ is lower than $\alpha_p = \text{Max}(z(\alpha))$ and αp^∞ (the conversion at the maximum point of DSC curves) is smaller than 0.632, which revealed that the two-parameter autocatalytic model could be used for both EP and EP/Sm-Fe₃O₄ nanocomposite [60,61].

$$y(\alpha) = \left(\frac{d\alpha}{dt}\right)_\alpha \exp\left(\frac{E_0}{RT_\alpha}\right) = Af(\alpha) \tag{6}$$

$$z(\alpha) = \left(\frac{d\alpha}{dt}\right)_\alpha T_\alpha^2, \tag{7}$$

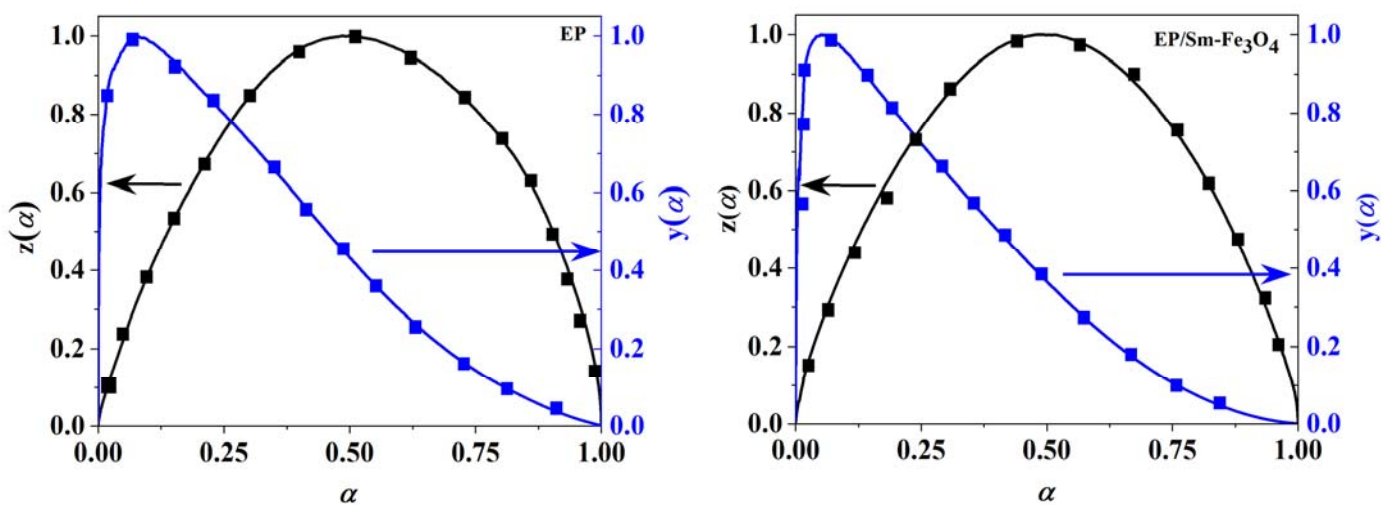


Figure 10. The shape and alteration pattern of $y(\alpha)$ and $z(\alpha)$ versus the extent of reaction captured by the Malek model.

Table 2. Malek parameters of EP and EP/Sm-Fe₃O₄.

Sample	Heating Rate (°C/min)	α_p	α_m	αp^∞
EP	2.5	0.447	0.075	0.497
	5	0.44	0.081	0.545
	7.5	0.482	0.087	0.553
	10	0.319	0.092	0.484
EP/Sm-Fe ₃ O ₄	2.5	0.456	0.051	0.487
	5	0.582	0.049	0.551
	7.5	0.429	0.05	0.51
	10	0.418	0.041	0.505

Therefore, the autocatalytic reaction model ($f(\alpha)$, Equation (8)) of neat epoxy and its nanocomposite were obtained by Friedman and Malek models.

$$f(\alpha) = \alpha^m(1 - \alpha)^n, \tag{8}$$

The reaction model parameters, including the pre-exponential factor ($\ln A$), non-catalytic (n), and autocatalytic (m) reaction orders, were determined from Equations (9) and (10) and Figure 11 and reported in Table 3.

$$\text{Value I} = \ln\left(\frac{d\alpha}{dt}\right) + \frac{E_\alpha}{RT} - \ln\left[\frac{d(1-\alpha)}{dt}\right] - \frac{E_\alpha}{RT'} = (n-m)\ln\left(\frac{1-\alpha}{\alpha}\right), \quad (9)$$

$$\text{Value II} = \ln\left(\frac{d\alpha}{dt}\right) + \frac{E_\alpha}{RT} + \ln\left[\frac{d(1-\alpha)}{dt}\right] + \frac{E_\alpha}{RT'} = (n+m)\ln(\alpha - \alpha^2) + 2\ln A, \quad (10)$$

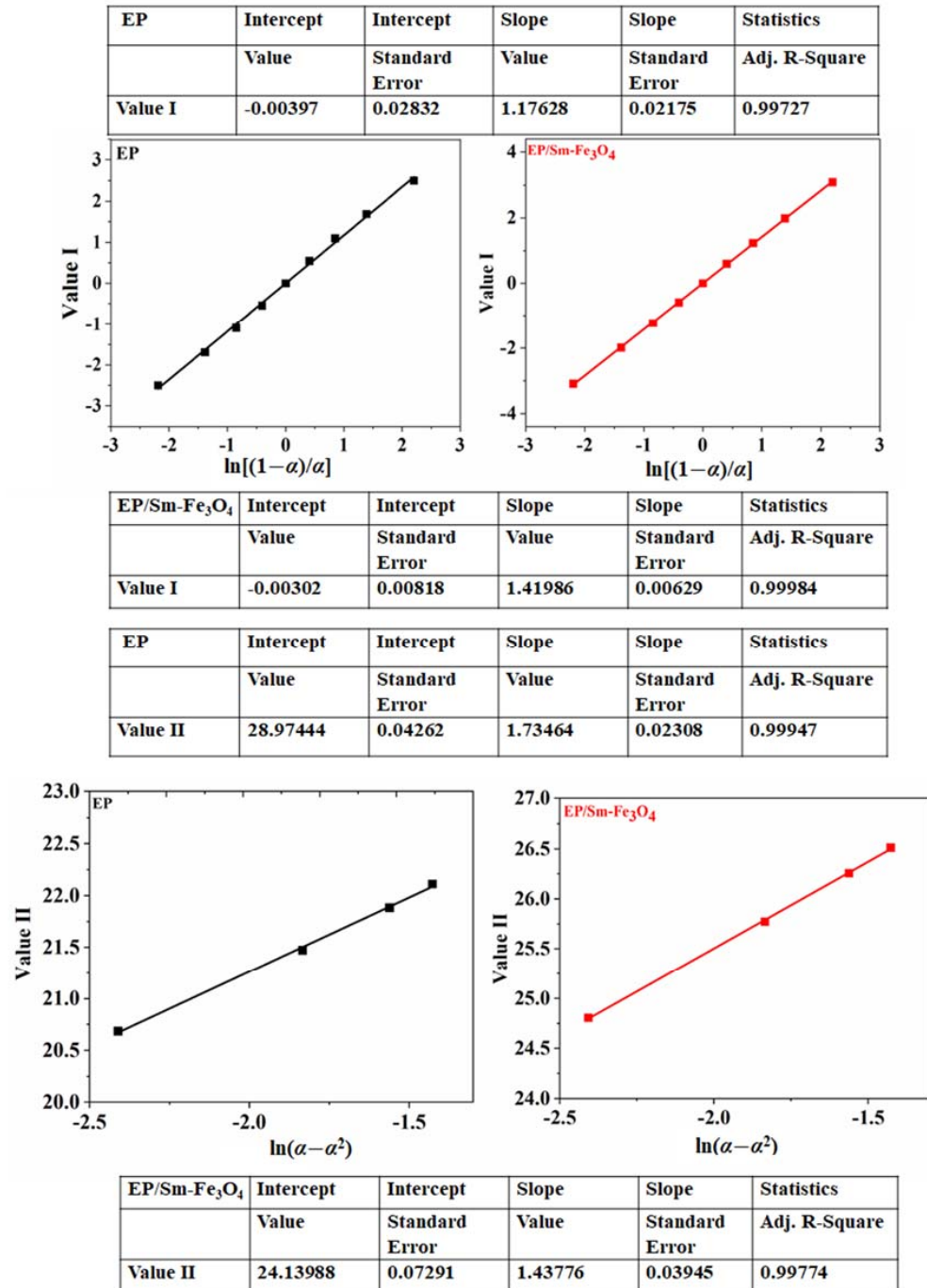


Figure 11. Value I and Value II for EP and EP/Sm-Fe₃O₄ nanocomposite.

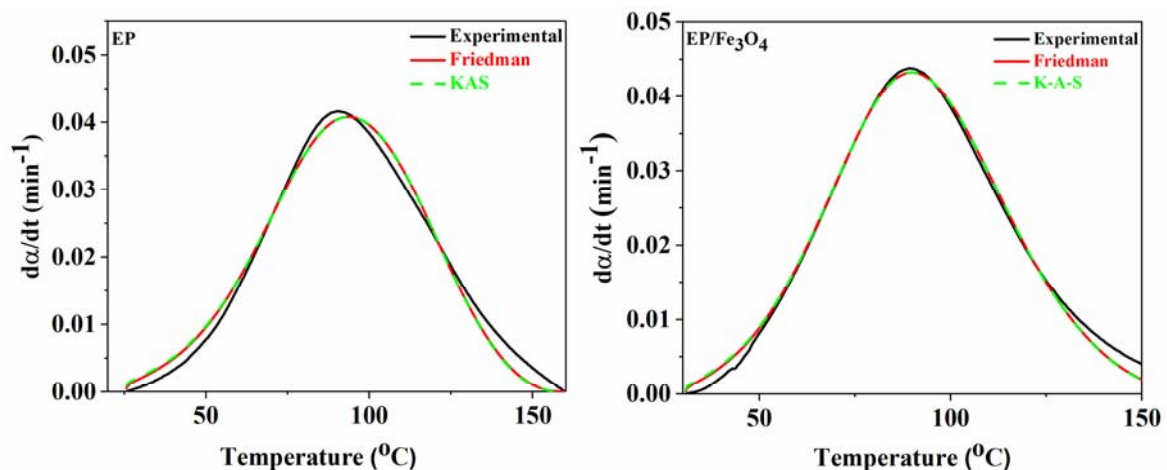
Table 3. The kinetic parameters evaluated for the curing of EP and EP/Sm-Fe₃O₄ nanocomposite based on Friedman and KAS models at different heating rates.

Designation	Heating Rate (°C/min)	Friedman			KAS		
		<i>m</i>	<i>n</i>	lnA (s ⁻¹)	<i>m</i>	<i>n</i>	lnA (s ⁻¹)
EP	2.5	0.14	1.32	12.09	0.09	1.36	13.3
	5.0	0.29	1.38	12.71	0.24	1.42	13.9
	7.5	0.29	1.36	12.76	0.24	1.4	13.92
	10	0.25	1.69	12.57	0.2	1.74	13.71
EP/Sm-Fe ₃ O ₄	2.5	0.16	1.58	14.5	0.13	1.62	15.39
	5.0	0.23	1.47	14.8	0.20	1.5	15.66
	7.5	0.34	1.72	15.05	0.30	1.75	15.9
	10	0.31	1.85	14.9	0.28	1.89	15.73

As can be observed, both *n* and *m* increased for EP/Sm-Fe₃O₄ nanocomposite compared to neat epoxy. An increment of *n* indicated the catalyzing effect of Sm³⁺ as a Lewis acid in the reaction between the epoxy ring and amine curing agent, and the enhancement of *m* is because of the reaction of OH groups on the surface of the Sm-Fe₃O₄ nanoparticles with epoxide rings. At a low heating rate (2.5 °C/min), the curing moieties have sufficient time to take part in cross-linking reactions at the early stage of curing reactions through chemically controlled reactions. At a high heating rate of 10 °C/min, the kinetic energy of the curing moieties is sufficiently high to facilitate a chemically control reaction as confirmed by a higher value of *n*. However, at medium heating rates ($\beta = 5$ and 7.5 °C/min), the *n* value may be decreased because of the absence of high kinetic energy and appropriate reaction time. The retardation effect of Sm-Fe₃O₄ nanoparticles on the cure reaction of epoxy is reflected in higher lnA values.

Validation of Isoconversional Methods

The validation of isoconversional methods (Friedman and KAS) is obtained by comparison with the experimental data and shown in Figure 12. Clearly, both KAS and Friedman approaches can predict the curing rate of the cross-linking reaction for neat epoxy and Sm-Fe₃O₄ nanoparticles incorporated epoxy systems.

**Figure 12.** Comparison of experimental data with the kinetic models for EP and EP/Sm-Fe₃O₄ nanocomposite based on Friedman and KAS model.

4. Conclusions

Sm-doped Fe₃O₄ nanoparticle was synthesized through an electrochemical method to investigate their effect on the curability of epoxy/amine system. XPS results indicated that samarium is present in its +3 oxidation states in the structure of Fe₃O₄ lattice. The XRD pattern revealed that Sm³⁺ ions occupy the octahedral sites in the Fe₃O₄ crystal structure.

DSC analysis at a different heating rate was performed to indicate Sm doping effect on the curing reaction of EP/Sm-Fe₃O₄ nanocomposites. It was found that the addition of Sm-Fe₃O₄ nanoparticles accelerates cross-linking reaction due to the catalyzing effect of Sm³⁺ in the crystal structure of Fe₃O₄ nanoparticles on the reaction between epoxy and amine curing agent, which is reflected in lower T_{Onset} and T_p . Obtaining Good CI by addition of Sm-Fe₃O₄ nanoparticles in epoxy matrix showed that Sm³⁺ participate in cross-linking of epoxy by catalyzing the reaction between epoxide rings and amine groups of the curing agent, and the etherification reaction of active OH groups on the surface of nanoparticles react with epoxy rings. The apparent activation energy determined by isoconversional Friedman and KAS methods indicated a complex curing reaction of epoxy in the presence of Sm-Fe₃O₄ nanoparticles, which caused an increase in average E_a value from 47.3 for neat epoxy to 52.6 kJ/mol. The autocatalytic reaction model was validated by experimental data. It can be concluded that doping Fe₃O₄ nanoparticles with Sm rare-earth element can enhance the surface active site of parent magnetic nanoparticles and enhance their dispersibility in the epoxy matrix and facilitate the cross-linking reaction of epoxy.

Author Contributions: Conceptualization, M.R.S.; methodology, M.J. and M.R.G.; software, M.J.; validation, M.J., and M.R.S.; formal analysis, M.J., M.M., and O.A.; investigation, K.J. and N.R.; data curation, S.H. and A.H.M.; writing—original draft preparation, M.J.; writing—review and editing, A.G.-P., F.J.S. and M.R.S.; visualization, M.J. and M.R.S.; supervision, M.R.S.; project administration, M.R.G. All authors have read and agreed to the published version of the manuscript.

Funding: This research received no external funding.

Institutional Review Board Statement: Not applicable.

Informed Consent Statement: Not applicable.

Data Availability Statement: Data are available upon request from the authors.

Conflicts of Interest: The authors declare no conflict of interest.

References

1. Yavuz, C.T.; Mayo, J.; William, W.Y.; Prakash, A.; Falkner, J.C.; Yean, S.; Cong, L.; Shipley, H.J.; Kan, A.; Tomson, M. Low-field magnetic separation of monodisperse Fe₃O₄ nanocrystals. *Science* **2006**, *314*, 964–967. [[CrossRef](#)]
2. Samal, S.; Kolinova, M.; Blanco, I. The magneto-mechanical behavior of active components in iron-elastomer composite. *J. Compos. Sci.* **2018**, *2*, 54. [[CrossRef](#)]
3. Yesmin, N.; Chalivendra, V. Electromagnetic Shielding Effectiveness of Glass Fiber/Epoxy Laminated Composites with Multi-Scale Reinforcements. *J. Compos. Sci.* **2021**, *5*, 204. [[CrossRef](#)]
4. Long, Y.; Chen, Z.; Duvail, J.L.; Zhang, Z.; Wan, M. Electrical and magnetic properties of polyaniline/Fe₃O₄ nanostructures. *Phys. B Condens. Matter* **2005**, *370*, 121–130. [[CrossRef](#)]
5. Roca, A.; Morales, M.; O’Grady, K.; Serna, C. Structural and magnetic properties of uniform magnetite nanoparticles prepared by high temperature decomposition of organic precursors. *Nanotechnology* **2006**, *17*, 2783. [[CrossRef](#)]
6. Samal, S.; Škodová, M.; Blanco, I. Effects of filler distribution on magnetorheological silicon-based composites. *Materials* **2019**, *12*, 3017. [[CrossRef](#)]
7. Bayat, M.; Yang, H.; Ko, F. Effect of iron oxide nanoparticle size on electromagnetic properties of composite nanofibers. *J. Compos. Mater.* **2018**, *52*, 1723–1736. [[CrossRef](#)]
8. Yao, D.; Peng, N.; Zheng, Y. Enhanced mechanical and thermal performances of epoxy resin by oriented solvent-free graphene/carbon nanotube/Fe₃O₄ composite nanofluid. *Compos. Sci. Technol.* **2018**, *167*, 234–242. [[CrossRef](#)]
9. Pathak, A.K.; Borah, M.; Gupta, A.; Yokozeki, T.; Dhakate, S.R. Improved mechanical properties of carbon fiber/graphene oxide-epoxy hybrid composites. *Compos. Sci. Technol.* **2016**, *135*, 28–38. [[CrossRef](#)]
10. Alexopoulos, N.D.; Paragkaman, Z.; Poulin, P.; Kourkoulis, S.K. Fracture related mechanical properties of low and high graphene reinforcement of epoxy nanocomposites. *Compos. Sci. Technol.* **2017**, *150*, 194–204. [[CrossRef](#)]
11. Yao, H.; Hawkins, S.A.; Sue, H.-J. Preparation of epoxy nanocomposites containing well-dispersed graphene nanosheets. *Compos. Sci. Technol.* **2017**, *146*, 161–168. [[CrossRef](#)]
12. Liu, X.; Xu, F.; Zhang, K.; Wei, B.; Gao, Z.; Qiu, Y. Characterization of enhanced interfacial bonding between epoxy and plasma functionalized carbon nanotube films. *Compos. Sci. Technol.* **2017**, *145*, 114–121. [[CrossRef](#)]
13. Sangermano, M.; Allia, P.; Tiberto, P.; Barrera, G.; Bondioli, F.; Florini, N.; Messori, M. Photo-Cured Epoxy Networks Functionalized With Fe₃O₄ Generated by Non-hydrolytic Sol–Gel Process. *Macromol. Chem. Phys.* **2013**, *214*, 508–516. [[CrossRef](#)]

14. Jouyandeh, M.; Rahmati, N.; Movahedifar, E.; Hadavand, B.S.; Karami, Z.; Ghaffari, M.; Taheri, P.; Bakhshandeh, E.; Vahabi, H.; Ganjali, M.R. Properties of nano-Fe₃O₄ incorporated epoxy coatings from Cure Index perspective. *Prog. Org. Coat.* **2019**, *133*, 220–228. [[CrossRef](#)]
15. Lakouraj, M.M.; Rahnaima, G.; Zare, E.N. Effect of functionalized magnetite nanoparticles and diaminoxanthone on the curing, thermal degradation kinetic and corrosion property of diglycidyl ether of bisphenol A-based epoxy resin. *Chin. J. Polym. Sci.* **2014**, *32*, 1489–1499. [[CrossRef](#)]
16. Nguyen, T.V.; Do, T.V.; Ha, M.H.; Le, H.K.; Le, T.T.; Nguyen, T.N.L.; Dam, X.T.; Vu, Q.T.; Dinh, D.A.; Dang, T.C. Crosslinking process, mechanical and antibacterial properties of UV-curable acrylate/Fe₃O₄-Ag nanocomposite coating. *Prog. Org. Coat.* **2020**, *139*, 105325. [[CrossRef](#)]
17. Jouyandeh, M.; Paran, S.M.R.; Khadem, S.S.M.; Ganjali, M.R.; Akbari, V.; Vahabi, H.; Saeb, M.R. Nonisothermal cure kinetics of epoxy/MnxFe₃-xO₄ nanocomposites. *Prog. Org. Coat.* **2020**, *140*, 105505. [[CrossRef](#)]
18. Jouyandeh, M.; Karami, Z.; Hamad, S.M.; Ganjali, M.R.; Akbari, V.; Vahabi, H.; Kim, S.-J.; Zarrintaj, P.; Saeb, M.R. Nonisothermal cure kinetics of epoxy/ZnxFe₃-xO₄ nanocomposites. *Prog. Org. Coat.* **2019**, *136*, 105290. [[CrossRef](#)]
19. Jouyandeh, M.; Ganjali, M.R.; Ali, J.A.; Akbari, V.; Karami, Z.; Aghazadeh, M.; Zarrintaj, P.; Saeb, M.R. Curing epoxy with polyethylene glycol (PEG) surface-functionalized GdxFe₃-xO₄ magnetic nanoparticles. *Prog. Org. Coat.* **2019**, *137*, 105283. [[CrossRef](#)]
20. Liu, J.; Bin, Y.; Matsuo, M. Magnetic behavior of Zn-doped Fe₃O₄ nanoparticles estimated in terms of crystal domain size. *J. Phys. Chem. C* **2012**, *116*, 134–143. [[CrossRef](#)]
21. Guo, M.; Balamurugan, J.; Li, X.; Kim, N.H.; Lee, J.H. Hierarchical 3D cobalt-doped Fe₃O₄ nanospheres@ NG hybrid as an advanced anode material for high-performance asymmetric supercapacitors. *Small* **2017**, *13*, 1701275. [[CrossRef](#)] [[PubMed](#)]
22. Groman, E.V.; Bouchard, J.C.; Reinhardt, C.P.; Vaccaro, D.E. Ultrasmall mixed ferrite colloids as multidimensional magnetic resonance imaging, cell labeling, and cell sorting agents. *Bioconjug. Chem.* **2007**, *18*, 1763–1771. [[CrossRef](#)]
23. Jouyandeh, M.; Ali, J.A.; Aghazadeh, M.; Formela, K.; Saeb, M.R.; Ranjbar, Z.; Ganjali, M.R. Curing epoxy with electrochemically synthesized Zn_xFe₃-xO₄ magnetic nanoparticles. *Prog. Org. Coat.* **2019**, *136*, 105246. [[CrossRef](#)]
24. Jouyandeh, M.; Ali, J.A.; Akbari, V.; Aghazadeh, M.; Paran, S.M.R.; Naderi, G.; Saeb, M.R.; Ranjbar, Z.; Ganjali, M.R. Curing epoxy with polyvinylpyrrolidone (PVP) surface-functionalized MnxFe₃-xO₄ magnetic nanoparticles. *Prog. Org. Coat.* **2019**, *136*, 105247. [[CrossRef](#)]
25. Jouyandeh, M.; Ganjali, M.R.; Ali, J.A.; Aghazadeh, M.; Karimzadeh, I.; Formela, K.; Colom, X.; Cañavate, J.; Saeb, M.R. Curing epoxy with ethylenediaminetetraacetic acid (EDTA) surface-functionalized CoxFe₃-xO₄ magnetic nanoparticles. *Prog. Org. Coat.* **2019**, *136*, 105248. [[CrossRef](#)]
26. Aghazadeh, M.; Ganjali, M.R. Samarium-doped Fe₃O₄ nanoparticles with improved magnetic and supercapacitive performance: A novel preparation strategy and characterization. *J. Mater. Sci.* **2018**, *53*, 295–308. [[CrossRef](#)]
27. Hoz, S. Samarium Iodide Showcase: Unraveling the Mechanistic Puzzle. *Acc. Chem. Res.* **2020**, *53*, 2680–2691. [[CrossRef](#)]
28. Ketteler, G.; Weiss, W.; Ranke, W.; Schlögl, R. Bulk and surface phases of iron oxides in an oxygen and water atmosphere at low pressure. *Phys. Chem. Chem. Phys.* **2001**, *3*, 1114–1122. [[CrossRef](#)]
29. Kim, T.Y.; Lee, M.S.; Kim, Y.I.; Lee, C.-S.; Park, J.C.; Kim, D. The enhanced anisotropic properties of the Fe₃-xMxO₄ (M= Fe, Co, Mn) films deposited on glass surface from aqueous solutions at low temperature. *J. Phys. D Appl. Phys.* **2003**, *36*, 1451. [[CrossRef](#)]
30. Cotton, S. *Lanthanide and Actinide Chemistry*; John Wiley & Sons: Hoboken, NJ, USA, 2013.
31. Kataby, G.; Ulman, A.; Cojocaru, M.; Gedanken, A. Coating a bola-amphiphile on amorphous iron nanoparticles. *J. Mater. Chem.* **1999**, *9*, 1501–1506. [[CrossRef](#)]
32. Tie, S.-L.; Lee, H.-C.; Bae, Y.-S.; Kim, M.-B.; Lee, K.; Lee, C.-H. Monodisperse Fe₃O₄/Fe@ SiO₂ core/shell nanoparticles with enhanced magnetic property. *Colloids Surf. A Physicochem. Eng. Asp.* **2007**, *293*, 278–285. [[CrossRef](#)]
33. De Silva, C.R.; Smith, S.; Shim, I.; Pyun, J.; Gutu, T.; Jiao, J.; Zheng, Z. Lanthanide (III)-doped magnetite nanoparticles. *J. Am. Chem. Soc.* **2009**, *131*, 6336–6337. [[CrossRef](#)]
34. Jouyandeh, M.; Tikhani, F.; Shabani, M.; Movahedi, F.; Moghari, S.; Akbari, V.; Gabrion, X.; Laheurte, P.; Vahabi, H.; Saeb, M.R. Synthesis, characterization, and high potential of 3D metal-organic framework (MOF) nanoparticles for curing with epoxy. *J. Alloys Compd.* **2020**, *829*, 154547. [[CrossRef](#)]
35. Karami, Z.; Jouyandeh, M.; Ali, J.A.; Ganjali, M.R.; Aghazadeh, M.; Maadani, M.; Rallini, M.; Luzi, F.; Torre, L.; Puglia, D.; et al. Cure Index for labeling curing potential of epoxy/LDH nanocomposites: A case study on nitrate anion intercalated Ni-Al-LDH. *Prog. Org. Coat.* **2019**, *136*, 105228. [[CrossRef](#)]
36. Jouyandeh, M.; Ganjali, M.R.; Ali, J.A.; Aghazadeh, M.; Stadler, F.J.; Saeb, M.R. Curing epoxy with electrochemically synthesized NixFe₃-xO₄ magnetic nanoparticles. *Prog. Org. Coat.* **2019**, *136*, 105198. [[CrossRef](#)]
37. Jouyandeh, M.; Zarrintaj, P.; Ganjali, M.R.; Ali, J.A.; Karimzadeh, I.; Aghazadeh, M.; Ghaffari, M.; Saeb, M.R. Curing epoxy with electrochemically synthesized GdxFe₃-xO₄ magnetic nanoparticles. *Prog. Org. Coat.* **2019**, *136*, 105245. [[CrossRef](#)]
38. Jouyandeh, M.; Karami, Z.; Ali, J.A.; Karimzadeh, I.; Aghazadeh, M.; Laoutid, F.; Vahabi, H.; Saeb, M.R.; Ganjali, M.R.; Dubois, P. Curing epoxy with polyethylene glycol (PEG) surface-functionalized NixFe₃-xO₄ magnetic nanoparticles. *Prog. Org. Coat.* **2019**, *136*, 105250. [[CrossRef](#)]
39. Jouyandeh, M.; Ganjali, M.R.; Ali, J.A.; Aghazadeh, M.; Stadler, F.J.; Saeb, M.R. Curing epoxy with electrochemically synthesized MnxFe₃-xO₄ magnetic nanoparticles. *Prog. Org. Coat.* **2019**, *136*, 105199. [[CrossRef](#)]

40. Akbari, V.; Jouyandeh, M.; Paran, S.M.R.; Ganjali, M.R.; Abdollahi, H.; Vahabi, H.; Ahmadi, Z.; Formela, K.; Esmaeili, A.; Mohaddespour, A.; et al. Effect of Surface Treatment of Halloysite Nanotubes (HNTs) on the Kinetics of Epoxy Resin Cure with Amines. *Polymers* **2020**, *12*, 930. [[CrossRef](#)]
41. Tikhani, F.; Moghari, S.; Jouyandeh, M.; Laoutid, F.; Vahabi, H.; Saeb, M.R.; Dubois, P. Curing Kinetics and Thermal Stability of Epoxy Composites Containing Newly Obtained Nano-Scale Aluminum Hypophosphite (AlPO₂). *Polymers* **2020**, *12*, 644. [[CrossRef](#)]
42. Jouyandeh, M.; Paran, S.M.R.; Jannesari, A.; Saeb, M.R. 'Cure Index' for thermoset composites. *Prog. Org. Coat.* **2019**, *127*, 429–434. [[CrossRef](#)]
43. Jouyandeh, M.; Ganjali, M.R.; Ali, J.A.; Aghazadeh, M.; Paran, S.M.R.; Naderi, G.; Saeb, M.R.; Thomas, S. Curing epoxy with polyvinylpyrrolidone (PVP) surface-functionalized Zn_xFe_{3-x}O₄ magnetic nanoparticles. *Prog. Org. Coat.* **2019**, *136*, 105227. [[CrossRef](#)]
44. Karami, Z.; Jouyandeh, M.; Ali, J.A.; Ganjali, M.R.; Aghazadeh, M.; Maadani, M.; Rallini, M.; Luzi, F.; Torre, L.; Puglia, D.; et al. Development of Mg-Zn-Al-CO₃ ternary LDH and its curability in epoxy/amine system. *Prog. Org. Coat.* **2019**, *136*, 105264. [[CrossRef](#)]
45. Karami, Z.; Jouyandeh, M.; Hamad, S.M.; Ganjali, M.R.; Aghazadeh, M.; Torre, L.; Puglia, D.; Saeb, M.R. Curing epoxy with Mg-Al LDH nanoplatelets intercalated with carbonate ion. *Prog. Org. Coat.* **2019**, *136*, 105278. [[CrossRef](#)]
46. Seidi, F.; Jouyandeh, M.; Akbari, V.; Paran, S.M.R.; Livi, S.; Ducos, F.; Vahabi, H.; Ganjali, M.R.; Saeb, M.R. Super-crosslinked ionic liquid-intercalated montmorillonite/epoxy nanocomposites: Cure kinetics, viscoelastic behavior and thermal degradation mechanism. *Polym. Eng. Sci.* **2020**, *60*, 1940–1957. [[CrossRef](#)]
47. Karami, Z.; Aghazadeh, M.; Jouyandeh, M.; Zarrintaj, P.; Vahabi, H.; Ganjali, M.R.; Torre, L.; Puglia, D.; Saeb, M.R. Epoxy/Zn-Al-CO₃ LDH nanocomposites: Curability assessment. *Prog. Org. Coat.* **2020**, *138*, 105355. [[CrossRef](#)]
48. Jouyandeh, M.; Ganjali, M.R.; Ali, J.A.; Aghazadeh, M.; Saeb, M.R.; Ray, S.S. Curing epoxy with polyvinylpyrrolidone (PVP) surface-functionalized Ni_xFe_{3-x}O₄ magnetic nanoparticles. *Prog. Org. Coat.* **2019**, *136*, 105259. [[CrossRef](#)]
49. Seidi, F.; Jouyandeh, M.; Paran, S.M.R.; Esmaeili, A.; Karami, Z.; Livi, S.; Habibzadeh, S.; Vahabi, H.; Ganjali, M.R.; Saeb, M.R. Imidazole-functionalized nitrogen-rich Mg-Al-CO₃ layered double hydroxide for developing highly crosslinkable epoxy with high thermal and mechanical properties. *Colloids Surf. A Physicochem. Eng. Asp.* **2021**, *611*, 125826. [[CrossRef](#)]
50. Jouyandeh, M.; Hamad, S.M.; Karimzadeh, I.; Aghazadeh, M.; Karami, Z.; Akbari, V.; Shammiry, F.; Formela, K.; Saeb, M.R.; Ranjbar, Z.; et al. Unconditionally blue: Curing epoxy with polyethylene glycol (PEG) surface-functionalized Zn_xFe_{3-x}O₄ magnetic nanoparticles. *Prog. Org. Coat.* **2019**, *137*, 105285. [[CrossRef](#)]
51. Calvino, M.M.; Lisuzzo, L.; Cavallaro, G.; Lazzara, G.; Milioto, S. Non-isothermal thermogravimetry as an accelerated tool for the shelf-life prediction of paracetamol formulations. *Thermochim. Acta* **2021**, *700*, 178940. [[CrossRef](#)]
52. Cavallaro, G.; Gallitto, A.A.; Lisuzzo, L.; Lazzara, G. Comparative study of historical woods from XIX century by thermogravimetry coupled with FTIR spectroscopy. *Cellulose* **2019**, *26*, 8853–8865. [[CrossRef](#)]
53. Sbirrazzuoli, N.; Vyazovkin, S. Learning about epoxy cure mechanisms from isoconversional analysis of DSC data. *Thermochim. Acta* **2002**, *388*, 289–298. [[CrossRef](#)]
54. Sbirrazzuoli, N.; Vyazovkin, S.; Mititelu, A.; Sladic, C.; Vincent, L. A study of epoxy-amine cure kinetics by combining isoconversional analysis with temperature modulated DSC and dynamic rheometry. *Macromol. Chem. Phys.* **2003**, *204*, 1815–1821. [[CrossRef](#)]
55. Jouyandeh, M.; Jazani, O.M.; Navarchian, A.H.; Shabaniyan, M.; Vahabi, H.; Saeb, M.R. Surface engineering of nanoparticles with macromolecules for epoxy curing: Development of super-reactive nitrogen-rich nanosilica through surface chemistry manipulation. *Appl. Surf. Sci.* **2018**, *447*, 152–164. [[CrossRef](#)]
56. Jouyandeh, M.; Jazani, O.M.; Navarchian, A.H.; Shabaniyan, M.; Vahabi, H.; Saeb, M.R. Bushy-surface hybrid nanoparticles for developing epoxy superadhesives. *Appl. Surf. Sci.* **2019**, *479*, 1148–1160. [[CrossRef](#)]
57. Jouyandeh, M.; Paran, S.M.R.; Shabaniyan, M.; Ghiyasi, S.; Vahabi, H.; Badawi, M.; Formela, K.; Puglia, D.; Saeb, M.R. Curing behavior of epoxy/Fe₃O₄ nanocomposites: A comparison between the effects of bare Fe₃O₄, Fe₃O₄/SiO₂/chitosan and Fe₃O₄/SiO₂/chitosan/imide/phenylalanine-modified nanofillers. *Prog. Org. Coat.* **2018**, *123*, 10–19. [[CrossRef](#)]
58. Karami, Z.; Ganjali, M.R.; Dehaghani, M.Z.; Aghazadeh, M.; Jouyandeh, M.; Esmaeili, A.; Habibzadeh, S.; Mohaddespour, A.; Inamuddin; Formela, K.; et al. Kinetics of Cross-Linking Reaction of Epoxy Resin with Hydroxyapatite-Functionalized Layered Double Hydroxides. *Polymers* **2020**, *12*, 1157. [[CrossRef](#)]
59. Jouyandeh, M.; Ganjali, M.R.; Seidi, F.; Xiao, H.; Saeb, M.R. Nonisothermal Cure Kinetics of Epoxy/Polyvinylpyrrolidone Functionalized Superparamagnetic Nano-Fe₃O₄ Composites: Effect of Zn and Mn Doping. *J. Compos. Sci.* **2020**, *4*, 55. [[CrossRef](#)]
60. Jouyandeh, M.; Karami, Z.; Paran, S.M.R.; Mashhadzadeh, A.H.; Ganjali, M.R.; Bagheri, B.; Zarrintaj, P.; Habibzadeh, S.; Vijayan P., P.; Saeb, M.R. Effect of Nickel Doping on the Cure Kinetics of Epoxy/Fe₃O₄ Nanocomposites. *J. Compos. Sci.* **2020**, *4*, 102. [[CrossRef](#)]
61. Moghari, S.; Jafari, S.H.; Yazdi, M.K.; Jouyandeh, M.; Hejna, A.; Zarrintaj, P.; Saeb, M.R. In-Out Surface Modification of Halloysite Nanotubes (HNTs) for Excellent Cure of Epoxy: Chemistry and Kinetics Modeling. *Nanomaterials* **2021**, *11*, 3078. [[CrossRef](#)]